

Imaging spectrometry at visible and infrared wavelengths using image replication

Andrew R Harvey^{1*}, David W Fletcher-Holmes¹, Sean S. Kudesia² and Ciaran Beggan²

¹School of Engineering and Physical Sciences, Heriot Watt University, Riccarton, Edinburgh, EH14 4AS UK

[*a.r.harvey@hw.ac.uk](mailto:a.r.harvey@hw.ac.uk)

²BAE SYSTEMS, GWW, Crewe Toll House, Ferry Road, Edinburgh, EH5 2XS, UK

ABSTRACT

We describe a new filter that simultaneously achieves spectral filtering and image replication to yield a two-dimensional, snapshot spectral imager. Filtering is achieved by spectral demultiplexing; that is without rejection of light; so optical throughput efficiency is, in principle, unity. The principle of operation can be considered as a generalisation of the Lyot filter to achieve multiple bandpasses. We report on the design and experimental implementation of an eight-band system for use in the visible and the design of an eight-band long-wave infrared system.

1. INTRODUCTION

Over the years many spectral imaging techniques have been described and it has become clear that all techniques involve some compromise with no single technique offering a panacea¹. The optimum technique can be determined by a comparison of the requirements for an application and the capabilities of candidate techniques. In this paper we describe a novel approach based on image replication and polarising interferometry that offers the important and fundamental advantages of snapshot spectral imaging in two dimensions. Dubbed IRIS², the technique enables 2D spectral imaging with moderate spectral resolution and an instantaneous field of view in pixels that is reduced in proportion to the number of spectral bands. To highlight the advantages offered by IRIS we will first discuss the limitations of traditional approaches to spectral imaging.

A fundamental aim of spectral imaging is to record a three-dimensional spectral-image cube (two transverse image dimensions and one spectral dimension) and a fundamental issue to be tackled is that this must be recorded using two-dimensional detector arrays. The solution to this dilemma is normally to time-sequentially record snapshot images of two of the spectral cube dimensions and to reconstruct the third dimension of the spectral data cube from *post hoc* assembly of the time-sequential data. Two pertinent examples are the use of a time-sequential filter wheel and the one-dimensional, pushbroom-scanned spectral imager¹. In the former case a time-sequential series of narrow-band images are recorded and subsequently coregistered and assembled into a spectral data cube. In the latter case, a time-sequential series of one-dimensional snapshot spectral images are recorded and reassembled to form a two-dimensional spectral image.

A major disadvantage of both techniques is that they are fundamentally unsuitable for recording phenomena that are changing on a timescale that is shorter than the duration required to reconstruct the data cube. Since this will typically be tens or hundreds of detector frames this is a major and fundamental restriction that imposes severe limitations in the application of spectral imaging to, for example, fast biochemical and combustion processes. Further problems arise when there is mutual translation between the scene to be spectrally imaged and the imager as occurs in spectral imaging of the eye^{3,4,5,6} and spectral imaging surveillance from aerial platforms^{7,8,9,10,11}. In both cases the major problem occurs because the translation is irregular and this can cause accurate coregistration of spectral images to be highly problematic. In the case where a one-dimensional image is scanned across the scene a penalty for imperfect coregistration is artefacts in the geometry of the spectral image, but for the case where the spectra are recorded in time sequence, imperfectly coregistered images introduce artefacts in the spectrum that reduce the effectiveness of spectral processing algorithms. In fact, to avoid this degradation typically requires coregistration of constituent images to be 1/20 of a pixel or better¹. This can be somewhat challenging. A major advantage of using a one-dimensional dispersive

spectral imager, as has been demonstrated in aerial hyperspectral surveillance and spectral imaging of the eye, is that this technique does not suffer from temporally induced spectral misregistration.

A further disadvantage of recording the spectral cube in time sequence is the reduced optical throughput: if N spectral filters are employed to time-sequentially record a spectral data cube during an integration time τ the integration time available for each narrow-band image is τ/N and the optical throughput is therefore reduced by a factor of N . For a push-broom-scanned one-dimensional spectral imager, a one-dimensional scene is recorded in a snapshot with, in principle, no multiplex loss, but to construct an image of $P \times Q$ pixels from Q such 1D images during an integration time τ means that the time available to record each 1D image is τ/Q . In this case the optical throughput is reduced by a factor Q .

For the IRIS technique described here the spectral data cube is recorded in a snapshot using a single detector array. This offers the following advantages:

- Time-resolved spectral imaging of transient phenomena is possible
- No temporally induced spectral misregistration or geometric distortion is introduced
- There are no multiplex losses so signal throughput can be very high
- There are no moving parts so reliability and robustness is high

The ability to record 2D snapshot spectral images is a fundamental advantage in terms of its ability to record transient or time-varying scenes, however the multiplex advantage depends upon the application. Fundamentally, the number of pixels in the spectral image cube (that is voxels) that can be recorded in a snapshot is limited by the space-bandwidth product (that is, the number of detector pixels) of the detector array or arrays that are used. The application of IRIS involves the snapshot imaging of N narrow-band non-overlapping images onto a single detector array so that there is a trade off between spectral resolution and field of view. Although, in terms of the number of pixels per image, the field of view of IRIS is reduced in comparison to a spectral imager using spectral-temporal multiplexing, if it is large enough without the need for spatial scanning for a particular application then there is a very significant multiplex advantage; as high as N in comparison to a spectrally multiplexed technique. If, however, a need for an extended field of regard requires scanning of the imager than this is in effect spatial multiplexing and the full multiplex advantage will not be obtained.

2. IMAGE REPLICATION IMAGING SPECTROMETER: PRINCIPLE OF OPERATION

The image replicating imaging spectrometer can be considered as a generalisation of a Lyot filter that enables spectral demultiplexing of broadband light. The Lyot filter^{12,13,14,15}, as used for many years in astronomy, employs polarising interferometry within multiple waveplates to yield a narrow-band filter suitable for recording monochromatic images. Light not transmitted by the Lyot filter is absorbed by film polarisers. To generalise the Lyot filter, Wollaston prism polarising beam splitters are used in place of film polarizers enabling spectral images to be recorded simultaneously in several pass-bands without rejection of light. To describe the principle of operation of IRIS we will first consider the principle of a conventional Lyot filter.

A Lyot filter, as illustrated in Figure 1, is composed of multiple waveplates sandwiched between co-aligned linear polarisers aligned to pass light polarised at 45° to the fast axis of each waveplate. The linearly polarised light propagating through the waveplate is resolved into orthogonally polarised components that interfere at the output analysing polariser with a mutual optical path difference $\Delta=(n_o-n_e)t$ between the orthogonal components where n_o and n_e are the ordinary and extraordinary refractive indices of the waveplate and t is its thickness. The output polariser is aligned with the input polariser so that the overall transmission function of the polariser-waveplate-polariser assembly is proportional to $\cos^2(\pi\nu\Delta)$ where $\nu=1/\lambda$ is optical frequency. A Lyot filter consists of an assembly of multiple polariser/waveplate combinations where the ratio between the thicknesses of consecutive waveplates is a factor of two. The spectral transmission function of an n -waveplate Lyot filter is thus the product of the transmission functions of all constituent waveplate/polariser assembly and is given by

$$T(\nu) = \prod_{i=1}^n \cos^2(i\pi\nu\Delta).$$

(1)

A four-waveplate Lyot filter is depicted in Figure 1. A generalisation of this technique is employed with the IRIS concept described here whereby the film polarisers are replaced with Wollaston prism polarising beam splitters as shown

in Figure 2 (a). The use of a polarising beam splitter means that after transmission through each waveplate the light is resolved into polarisations both, aligned with, and orthogonal to, the input polarisation state. As with the Lyot filter, for the co-polarised component the transmission function is given by $\cos^2(\pi\nu\Delta)$; for the cross-polarised component the transmission function is $\sin^2(\pi\nu\Delta)$. Furthermore, these two orthogonally polarised components are displaced in angle by the beam-splitting action of the Wollaston prism and this enables two spatially separated and spectrally filtered replica images to be formed. Subsequent Wollaston prism polariser pairs further spectrally filter and replicate the images. After transmission through n Wollaston prism polariser pairs 2^n replicated images are formed, each with a unique product of $\sin^2(i\pi\nu\Delta)$ and $\cos^2(i\pi\nu\Delta)$ transmission functions. It can be seen then that the IRIS technique simultaneously replicates the image formed at the field stop whilst applying a unique spectral filtering function to each image; this filtering function is determined by how light arriving at each image was steered and spectrally modulated. IRIS thus performs the function of an imaging spectral demultiplexor with image components lying within a spectral band tending to be steered to a particular part of the detector array. The images at the detector array are prevented from overlapping by the field stop.

The orientation and magnitude of the splitting angles of the splitting angles of the Wollaston prisms determines the locations of the replicated images at the detector; each image can be identified by a vector $\{p(1), p(2).. p(n)\}$ where each element of the vector identifies whether the image is due to refraction in a positive or negative direction at each Wollaston prism. In general, the transmission function for each image at location $\{p(1), p(2).. p(n)\}$ in the image plane can be written as

$$T_{p(1),p(2)..p(n)}(\nu) = \prod_{i=1}^n \Omega_{a(i)}(i\pi\nu\Delta) \quad (2)$$

where $a(i)$ refers to either co-polar or cross-polar transmission between Wollaston prisms, so that the respective transmission functions for co-polar and cross-polar transmissions through waveplate i sandwiched between polarisers $i-1$ and i are

$$\begin{aligned} \Omega_{a(i)=co-polar}(x) &= \cos^2(x), \\ \Omega_{a(i)=cross-polar}(x) &= \sin^2(x) \end{aligned} \quad (3)$$

where suffix $i=0$ indicates the input polarizer and all other values indicate Wollaston prism polarizers. The spectrum associated with each individual image replication is determined by the vector $\{a(1), a(2).. a(n)\}$ appropriate for each image replication. Since spectral filtering and image replication operations commute, the order of the vector elements is not important; it will always result in the same combination of 2^n products of the n pairs of \cos^2 and \sin^2 functions being applied at the image. For an IRIS employing three Wollaston prisms the eight pass-bands pass-band are given by

$$\begin{aligned} T_1(\nu) &= \cos^2[\pi\nu\Delta]\cos^2[2\pi\nu\Delta]\cos^2[4\pi\nu\Delta] \\ T_2(\nu) &= \cos^2[\pi\nu\Delta]\cos^2[2\pi\nu\Delta]\sin^2[4\pi\nu\Delta] \\ T_3(\nu) &= \cos^2[\pi\nu\Delta]\sin^2[2\pi\nu\Delta]\cos^2[4\pi\nu\Delta] \\ T_4(\nu) &= \cos^2[\pi\nu\Delta]\sin^2[2\pi\nu\Delta]\sin^2[4\pi\nu\Delta] \\ T_5(\nu) &= \sin^2[\pi\nu\Delta]\cos^2[2\pi\nu\Delta]\cos^2[4\pi\nu\Delta] \\ T_6(\nu) &= \sin^2[\pi\nu\Delta]\cos^2[2\pi\nu\Delta]\sin^2[4\pi\nu\Delta] \\ T_7(\nu) &= \sin^2[\pi\nu\Delta]\sin^2[2\pi\nu\Delta]\cos^2[4\pi\nu\Delta] \\ T_8(\nu) &= \sin^2[\pi\nu\Delta]\sin^2[2\pi\nu\Delta]\sin^2[4\pi\nu\Delta] \end{aligned} \quad (4)$$

As can be seen the first term is identical to the spectral transmission function of the equivalent Lyot filter. Due to the wide spectral range of IRIS it is necessary to use the dispersive variation of Δ with wavenumber when evaluating (4). In Figure 3(a) are shown the eight calculated transmission functions for an eight-band IRIS employing quartz waveplates with thicknesses for the three waveplates of $t=120, 240$ and $480 \mu\text{m}$. The resultant pass-bands are bell-shaped and

exhibit significant sidelobes. For visible band imaging, quartz is an ideal material for the waveplates since its relatively small birefringence yields relatively thick and robust waveplates with relaxed manufacturing tolerances.

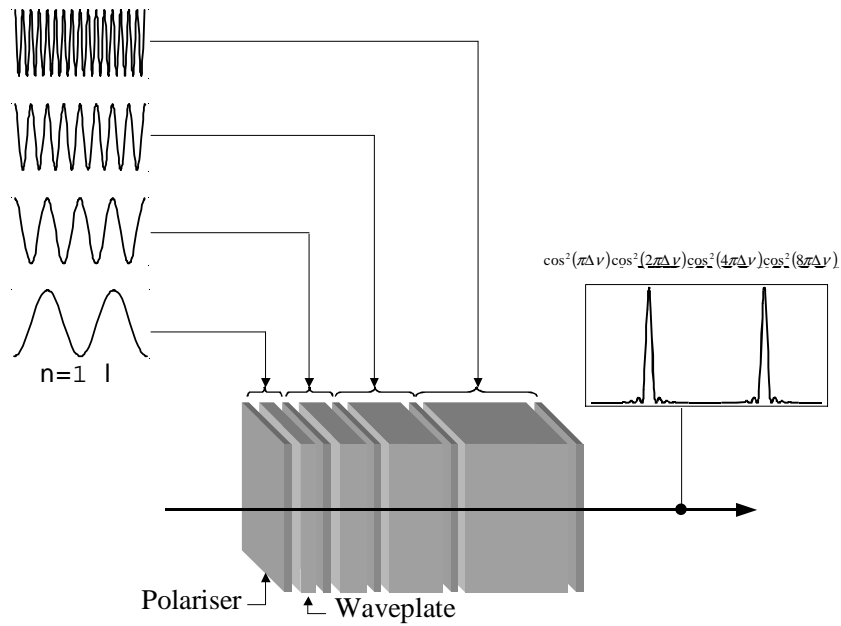


Figure 1 Depiction of the principle of operation of the Lyot filter

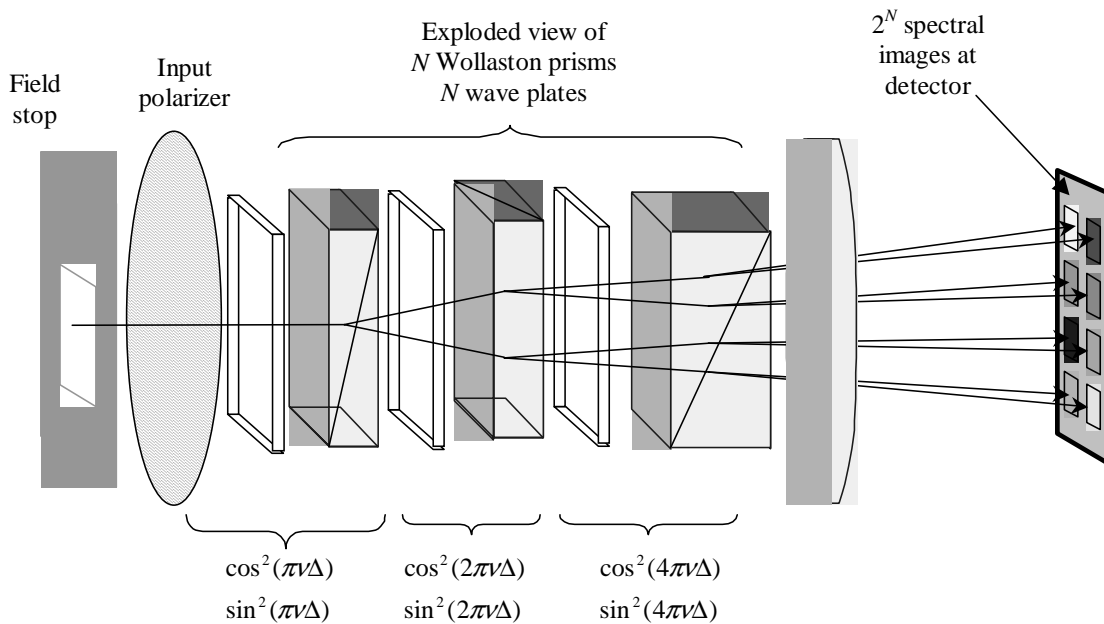


Figure 2 Depiction of principle of operation of Image replication imaging spectrometer

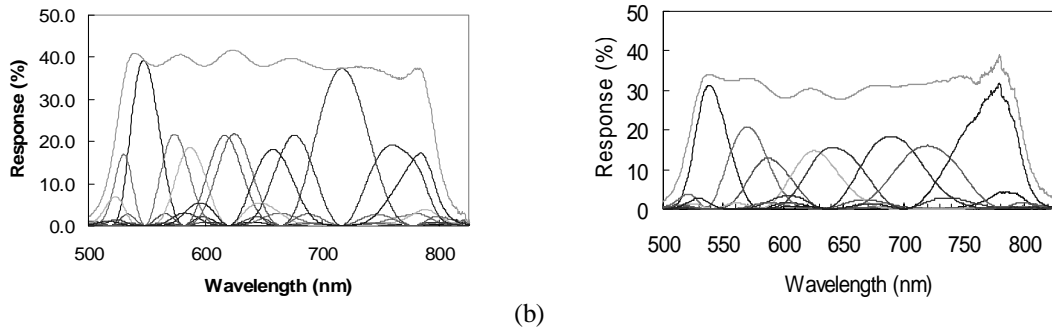


Figure 3 Transmission functions for each of eight images using (a) theoretical transmission for waveplates related by a simple factor of 2 and (b) measured transmission for waveplates optimised in thickness to produce transmission curves with maximum fractional power in the main lobes.

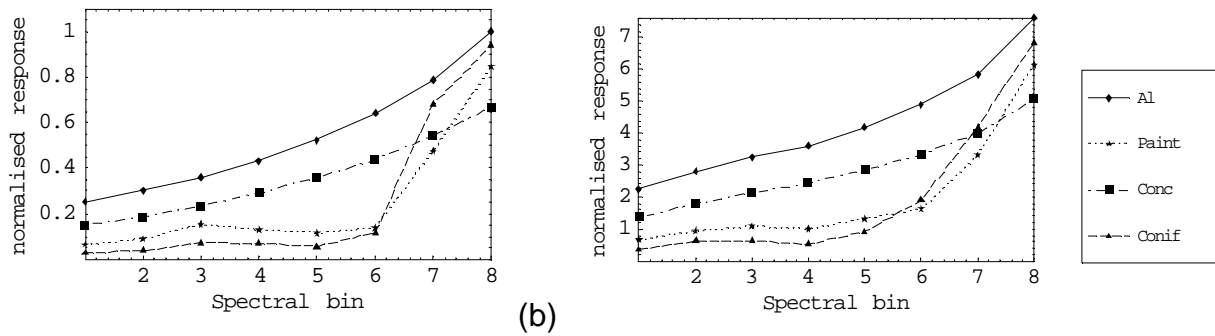


Figure 4 Spectral characterisation of spectra of aluminium, green paint, concrete and coniferous vegetation convolved with (a) rectangular filter functions and (b) IRIS optimised filter functions.

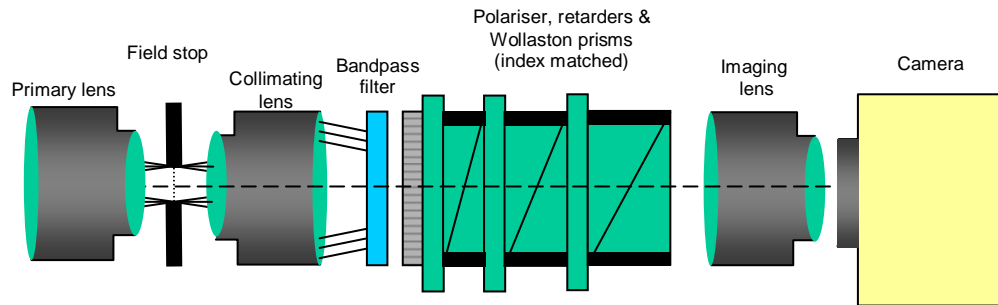


Figure 5 (a) Schematic of the implementation of the 8-channel IRIS concept within a spectral imager

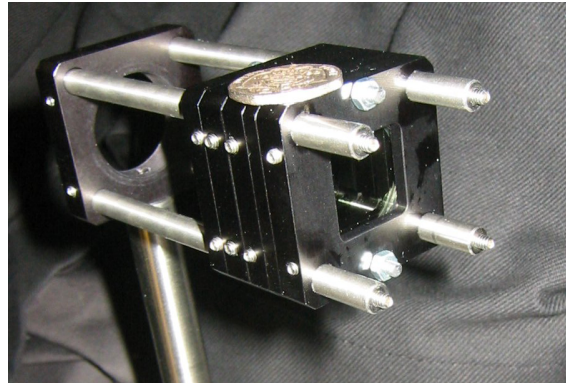


Figure 6 Assembled Wollaston prisms and waveplates for an 8-channel IRIS

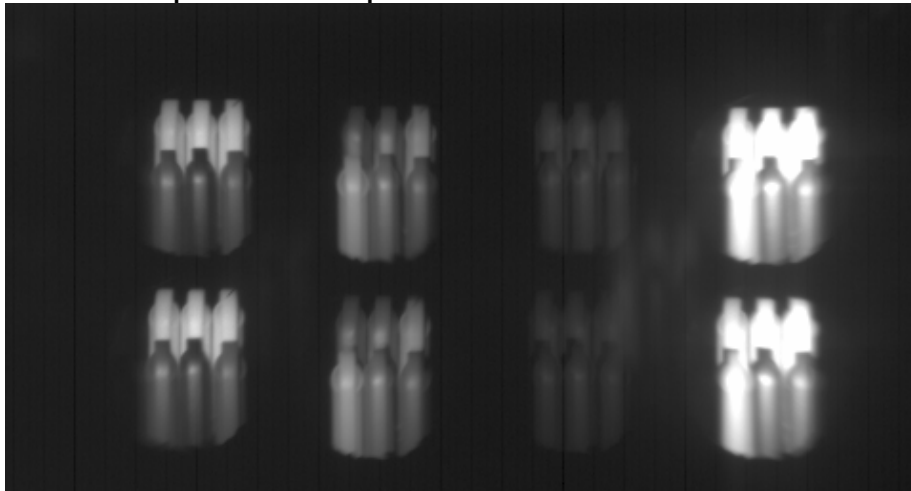


Figure 7 Replicated images of six different coloured pens at the detector plane of IRIS.

Modification of the thicknesses of the waveplates can improve the characteristics of the passbands; optimisation of the thickness values against a merit function related to the desired spectral filtering characteristics can suppress the sidelobes. We have found that a merit function that maximises the average optical power in the main peaks of each transmission function (and hence minimising the average sidelobe power) yields spectral curves that are efficient at maximising the separation of the spectra of typical materials in spectral hyperspace. It is more appropriate then to replace equation (3) by

$$\Omega_{a(i)}(\nu) = \cos^2(\pi\nu b(\nu)t_i)$$

$$\Omega_{s(i)}(\nu) = \sin^2(\pi\nu b(\nu)t_i)$$

(5)

where t_i is the thickness of waveplate i and $b(\nu)$ is the birefringence at wavenumber ν .

Optimisation of the above system using this technique yielded thicknesses for the quartz waveplates of $t=121$, 176 and $350 \mu\text{m}$. Measured transmission functions under polarised illumination for an optimised eight band imager, based on these thicknesses are shown in Figure 3(b). The spectral transmission is restricted by low-pass and high-pass edge filters. The overall transmission efficiency of this system is limited to about 45% in polarised light; the dominant contributions arise from the dichroic input polariser and losses in the two edge filters. The use of a high efficiency single element bandpass filter will increase transmission to greater than 80%.

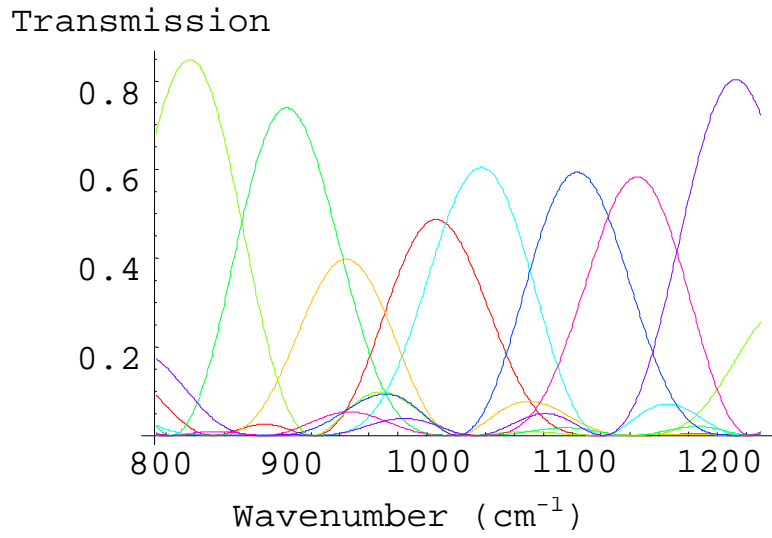


Figure 8 Transmission functions for an 8-band IRIS system employing cadmium selenide waveplates.

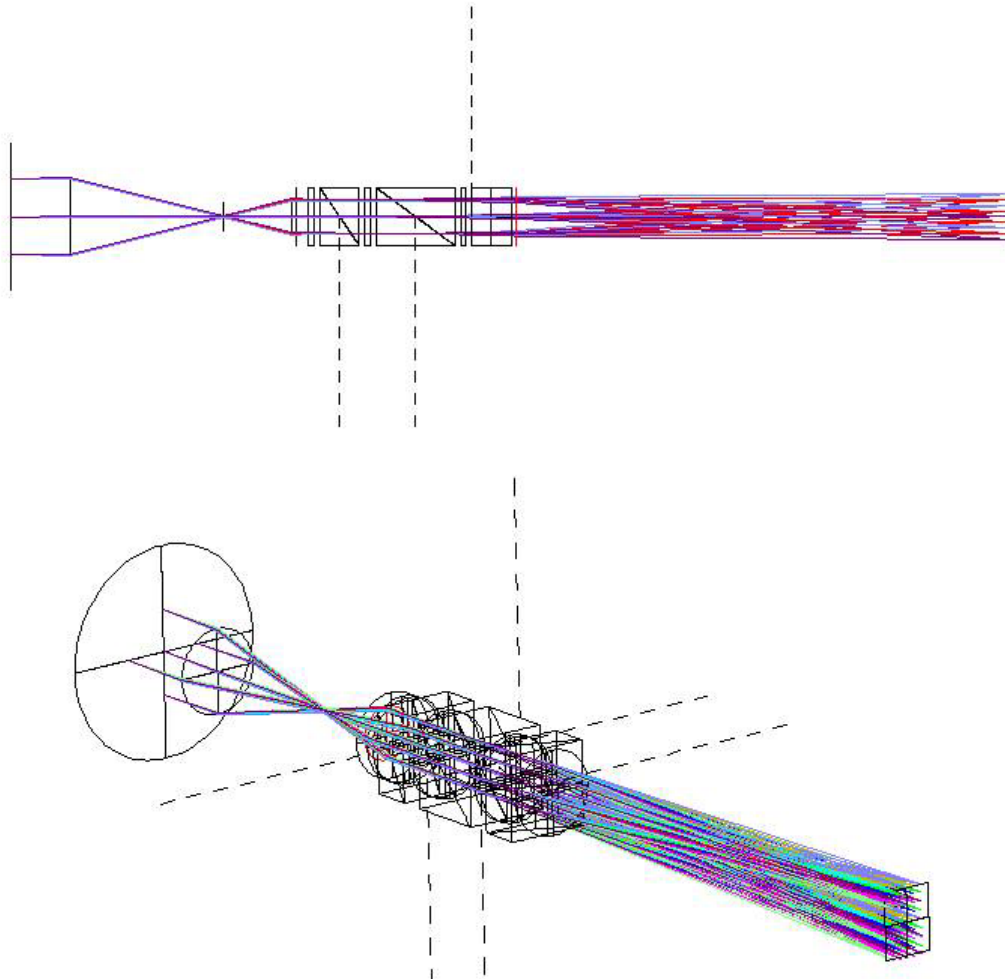


Figure 9 Ray trace of 8-channel IRIS system based on CdSe birefringent components.

Whilst it is not possible to synthesis the contiguous rectangular functions typically employed in spectrometry, in many cases this will not significantly reduce spectral discrimination performance of IRIS. A heuristic illustration of this is the good spectral discrimination possible with the human visual system which also employs broad overlapping and bell-shaped response curves. A more quantitative appraisal is the evaluation of the separation of recorded spectra in spectral space. For example, in Figure 4 is shown the relative energy in each spectral bin when the spectra of aluminium, green paint, concrete and coniferous vegetation are convolved with rectangular response functions and also when the spectra are convolved with the response functions of a typical IRIS. The total intensities in each bin are normalised to that of aluminium in band 8 when rectangular contiguous filters are used. Perhaps the most striking feature is that the intensity at the detectors is eight-fold higher for IRIS than for a conventional time-sequential systems.

On the other hand, the bell-shaped responses of IRIS have resulted in some smoothing of the recorded spectra. In practice, the ability to discriminate between spectra is determined by both the separation of these spectra in eight-dimensional spectral space and the noise contribution at each point. In this example, the mean reduction in separation of the spectra in spectral space is 8%, whilst the signal level is increased by a factor of eight, consequently for detector-noise limited imaging, IRIS offers a 7.4-fold improvement in signal-to-noise ratio over an ideal time-sequential spectral imager.

3. EXAMPLE RESULTS FOR A VISIBLE-BAND IRIS

A schematic of an assembled, 8-channel IRIS system is shown in Figure 5. This consists of an image relay system with an intermediate image plane. The IRIS components depicted in figure 3 are located close to the pupil plane of the image relay system, thus they replicate the image formed at the field stop onto the detector array. The field stop, or intermediate focal plane, is required to prevent overlapping of the replicated images at the detector plane. The IRIS birefringent elements are assembled into a common block with index matching fluid to reduce stray reflections and to reduce the effect of non-flatness of the birefringent elements. A photograph of the assembled IRIS block is shown in Figure 6 with together a UK 20p coin for scale.

As an example of the images recorded by IRIS, we show in Figure 7 the replicated images formed at the detector plane for an input scene consisting of six coloured pens. The variations of the grey levels for each pen in the eight images is due to the spectral filtering functions of the IRIS system. The spectral image cube is constructed by coregistration of these eight bandpass images. There are some aspects of this process that require calibration, including small amounts of fixed distortion introduced by the lens and a small amount of image smear introduced by dispersion in the Wollaston prism birefringence. Although we have demonstrated the IRIS technique in the visible band, we have identified birefringent materials that will enable its applications across a wide range of wavelengths between 200 nm and 15 μm . The design of a thermal infrared IRIS is described in the next section.

4. DESIGN OF A THERMAL INFRARED IRIS

For application in the thermal infrared, the design of IRIS follows the same principles as in the visible, although the availability of materials and considerations of stray light and cold-shielding introduce significant added complexity, particularly in the 8-12 μm band. Several materials exist that enable operation across all or part of the 3-14 μm range of interest to thermal imaging. Criteria to be considered in selecting materials include issues such as field of view, the shape of the passbands, the degree of smearing due to dispersion in the birefringence and practicalities of prism manufacture and system integration. An example set of optimised transmission bands to cover the 8-12 μm range is shown in Figure 8 for CdSe waveplates. A ray trace of a LWIR system employing CdSe waveplates and Wollaston prisms is shown in Figure 9.

5. CONCLUSIONS

We have described a new concept in spectral imaging instrumentation that combines polarising interferometry and polarising beam splitters to simultaneously implement image replication and spectral demultiplexing. This enables snapshot spectral imaging in two dimensions, promising the extension of spectral imaging to transient phenomena and imaging from unstable platforms. Moreover, in contrast to other high throughput techniques, such as Fourier-transform spectroscopy¹, there is no data inversion and so the associated SNR advantage is retained even in shot-noise limited imaging conditions.

6. ACKNOWLEDGEMENTS

This work was carried out with funding from Sensors and Electronic Warfare Research Domain of the UK MoD Corporate Research Programme, BAE systems and The Royal Society.

7. REFERENCES

- ¹ A.R. Harvey, J. Beale, A.H. Greenaway, T.J. Hanlon and J. Williams, "Technology options for imaging spectrometry" *Proc SPIE*, 4132, pp13-24, 2000
- ² A R Harvey, D W Fletcher-Holmes, *Imaging apparatus*, GB Patent application 0215248.6, 2nd July 2002.
- ³ A.R.Harvey, J.Lawlor, A.I.McNaught, J.W.Williams and D.W.Fletcher-Holmes. *Hyperspectral imaging for the detection of retinal diseases*. SPIE 4816-37, pp325-335, Proc. Conference on Imaging Spectrometry VIII, Seattle July 7-11, 2002.
- ⁴ V.Papadakis, M.P. Karavellas, M.K. Tsillimbaris, C.Balas, and I.G.Pallikaris, *A hyperspectral imaging fundus camera for the detection and characterisation of retinal lesions*. The Association for Research in Vision and Ophthalmology. Ocular Imaging, 4362-B331, pp. 174, May 5-10, 2002.
- ⁵ J.Lawlor, D.W.Fletcher-Holmes A.I.McNaught A.R.Harvey. *In vivo hyperspectral imaging of human retina and optic disc*. The Association for Research in Vision and Development, Anatomy and Physiology/Retinal Cell Biology. 4350-B319. Annual Meeting Fort Lauderdale, Florida May 5-10, 2002
- ⁶ F. C.Delori, *Spectrophotometer for noninvasive measurement of intrinsic fluorescence and reflectance in the ocular fundus*, Applied Optics, Vol. 33, pp.7439-7452, 1994.
- ⁷ P Mouroulis, *Spectral and spatial uniformity in push-broom imaging spectrometers*, Imaging spectrometry V, SPIE 3753 pp 133-141 (1999)
- ⁸ G R O Vane, T G Green, H T Chrien, E G Hanson, W M Porter,*The airborne visible/infrared imaging spectrometer (AVRIS)* Remote Sen. Environ., **44**, pp127-143, (1993)
- ⁹ T Wilson, C Davis, *Naval EarthMap Observer (NEMO) Satellite*, Imaging Spectrometry V, SPIE 3753, pp 2-11 (1999)
- ¹⁰ J A Hackwell et al, *LWIR/MWIR imaging hyperspectral sensor for airborne and ground-based remote sensing*, Proc. SPIE 2819, pp 274-283 (1995)
- ¹¹ R W Basedow, D C Carmer, M L Anderson, *HYDICE system implementation and performance*, SPIE 2480, pp 258-267 (1995)
- ¹² B. Lyot, *Filter monochromatique polarisant et ses applications en physique solaire*, Ann. Astrophys. 7, 32 (1944)
- ¹³ B. Lyot, *Optical apparatus with wide field using interference of polarized light*, C.R. Acad. Sci. (Paris) 197, 1593 (1933).
- ¹⁴ Y. Ohman, *A new monochromator*, Nature 41, 157, 291 (1938).
- ¹⁵ Y. Ohman, *On some new birefringent filter for solar research*, Ark. Astron. 2, 165 (1958).